PLOS ONE

RESEARCH ARTICLE

Embankment seismic fragility assessment: A case study on Xi'an-Baoji expressway (China)

Fa Che[1], **Chao Yin**[2,3,4]*, **Xingkui Zhao**[5], **Zhinan Hu**[4], **Lu Sheng**[5], **Dong Liu**[6]

1 Zibo Transportation Service Center, Zibo, China, **2** School of Civil and Architecture Engineering, Shandong University of Technology, Zibo, China, **3** Key Laboratory of Roads and Railway Engineering Safety Control (Shijiazhuang Tiedao University), Ministry of Education, Shijiazhuang, China, **4** State Key Laboratory of Mechanical Behavior and System Safety of Traffic Engineering Structures, Shijiazhuang Tiedao University, Shijiazhuang, China, **5** Shandong Dongtai Engineer Consulting Co., LTD., Zibo, China, **6** Laoling Branch of Dezhou Highway Development Center, Dezhou, China

* yinchao1987611@163.com

Citation: Che F, Yin C, Zhao X, Hu Z, Sheng L, Liu D (2021) Embankment seismic fragility assessment: A case study on Xi'an-Baoji expressway (China). PLoS ONE 16(2): e0246407. https://doi.org/10.1371/journal.pone.0246407

Editor: Hao Sun, Northeastern University, UNITED STATES

Received: August 8, 2020

Accepted: January 19, 2021

Published: February 5, 2021

Data Availability Statement: All relevant data are within the manuscript and its Supporting information files.

Funding: This work was supported by the National Natural Science Foundation of China (Grant NO. 51808327) and Natural Science Foundation of Shandong Province (Grant NO. ZR2019PEE016), awarded to author CY. Zibo Transportation Service Center is a commercial organization and provided support in the form of salary for FC. Shandong Dongtai Engineer Consulting Co., LTD. is also a commercial organization and provided support in

Abstract

Although embankment seismic damages are very complex, there has been little seismic fragility research yet. Researches on seismic fragility of bridges, dams and reinforced concrete (RC) structures have achieved fruitful results, which can provide references for embankment seismic fragility assessment. Meanwhile, the influencing degrees of retaining structures, such as retaining walls on the embankment seismic performances are still unclear. The K1025+470 embankment of the Xi'an-Baoji expressway was selected as the research object, and the finite difference models of the embankment fill-soil foundation system and embankment fill-soil foundation-retaining wall system were established. The ground-motion records for Incremental Dynamic Analysis (IDA) were selected and the dynamic response analysis were conducted. Probabilistic Seismic Demand Analysis (PSDA) was used to deal with the IDA results and the seismic fragility curves were generated. Based on the assessment results, the influences of the retaining wall on the embankment seismic fragility were further verified. The research results show that regardless of which seismic damage parameter is considered or the presence or absence of the retaining wall, larger PGAs always correspond to higher probabilities of each seismic damage grade. Seismic damages to the embankment fill-soil foundation-retaining wall system are always lower than those of the embankment fill-soil foundation system under the same PGA actions, thus, the retaining wall can decrease the embankment seismic fragility significantly.

1 Introduction

Earthquakes are natural disasters occur in bursts and severely endanger people's lives and properties [1]. The 1976 Tangshan earthquake in Hebei, China, the 1999 Chi-Chi earthquake in Taiwan, China, the 2008 Wenchuan earthquake in Sichuan, China, the 2010 earthquakes in Haiti and Chile, and the 2011 earthquake of the Pacific coast of Tōhoku in Japan and other previous violent earthquakes, highway embankments suffered from varying degrees of damages, which seriously disrupted the highway networks, becoming the "Gordian knots" for the

the form of salary for XZ and LS. Laoling Branch of Dezhou Highway Development Center is not a commercial organization, but provided funding to author DL. The funders had no role in study design, data collection and analysis, decision to publish, or preparation of the manuscript. The specific roles of all authors were articulated in the "author contributions" section.

Competing interests: Zibo Transportation Service Center is a commercial organization and provided support in the form of salary for Fa Che. This affiliation does not alter our adherence to PLOS ONE policies on sharing data and materials. There are no patents, products in development or marketed products to declare.

whole earthquake relief work [2–5]. Embankment seismic fragility refers to the exceeding probabilities of different damage grades under earthquake actions, it can not only describe the relations between the ground-motion intensities and embankment damage grades, but also portray the embankment seismic performances [6–8]. The assessment results of the embankment seismic fragility can be used as the basis for embankment design and engineering fortification, suggesting reasonable options for improving highway seismic capacities [9–11].

Seismic fragility assessment started with the nuclear power plant, and reflected the results with the fragility curves and/or fragility matrixes [12–14]. A. Melani et al. [15] determined the financial risks on the basis of results of Incremental Dynamic Analysis (IDA) of reinforced concrete (RC) frames using nonlinear time history analyses with a suite of 20 ground motion records. Wang et al. [16] investigated the seismic fragility of arch dams using the dynamic damage analysis model of dam-reservoir-foundation systems, in which the radiation damping of semi-unbounded foundation rock, opening of contraction joints and damage cracking of dam concrete were taken into account. Ko and Yang [17] performed nonlinear finite element analyses using PLAXIS 2D for the seismic responses of sheet-pile wharves, and the modeling approach was verified to be satisfactory by simulating a 1-g scale-model shaking table test. Liu et al. [18] performed the seismic fragility analysis of recycled aggregate concrete (RAC) bridge columns with different recycled coarse aggregate (RCA) replacement ratios subjected to freeze-thaw cycles (FTCs) by the cloud analysis method. Yoon et al. [19] carried out nonlinear time history analyses for the pipeline considering soil-pipeline interaction represented by beam on nonlinear Winkler foundation model, and 12 ground motions were employed and four different analytical cases were considered to evaluate the effect of the uncertainty of soil parameters. Bao et al. [20] used both as-recorded and artificial seismic sequences as input to conduct the nonlinear dynamic analysis, and the effect of fault types of aftershocks on a mainshock-damaged containment was investigated in terms of the global response and local damage respectively. Chen et al. [21] used a small-scale shaking table model test to investigate the characteristics of the granular landslide deposits under influences of seismic wave, the results showed that vibration frequency significantly influenced the deposit shape. Pan et al. [22] employed the Latin hypercube sampling (LHS) technique to generate random samples of different uncertain parameters, and IDA was carried out to establish probabilistic seismic demand models (PSDMs) and develop fragility curves. Sainct et al. [23] proposed a methodology based on Support Vector Machine (SVM) coupled with an active learning algorithm to estimate fragility curves. Sarno and Pugliese [24] assessed the seismic fragility of typical existing RC structures subjected to earthquake sequences and various levels of corrosion, and a probabilistic approach and three different seismic intensity measures (IM) were proposed. Liang et al. [25] performed the approximate IDA and the slippage and sliding area ratio were chosen as the engineering demand parameters (EDPs), and different damage levels were identified by the slippage-based rule and sliding area ratio-based rule respectively according to their corresponding overall mean IDA curves. Kumar and Samanta [26] determined the lognormal variability functions by accounting for both the aleatory uncertainties and epistemic source uncertainties, and seismic fragility assessment was performed for different building categories in Patna, India. Ciano et al. [27] investigated the accuracy of fragility curves for an actual building struck by the 2016 Italian earthquake, and numerical analyses considering both linear and non-linear behavior of a multi-degree of freedom structural system subjected to this earthquake were performed. Ebrahimi et al. [28] used a number of effective techniques including LHS simulation, fuzzy set theory and α-cut approach to quantify the median of the collapse fragility curve as the fuzzy-random response. Ding et al. [29] conducted a series of shaking table tests of utility tunnels with and without a joint connection, the results showed that the

structure without a joint connection presented a more significant acceleration response and horizontal soil pressure response than those with a joint connection.

Although embankment seismic damages are very complex, there has been little seismic fragility research yet. Researches on seismic fragility of bridges, dams and RC structures have achieved fruitful results, which can provide references for embankment seismic fragility assessment. Meanwhile, the influencing degrees of retaining structures, such as retaining walls on the embankment seismic performances are still unclear [7, 30]. In view of this, seismic fragility assessment of the K1025+470 embankment of the Xi'an-Baoji expressway was performed by IDA and Probabilistic Seismic Demand Analysis (PSDA), and fragility curves were generated. Based on the assessment results, the influences of the RC retaining wall on the embankment seismic fragility were further verified.

2 Methodology

Embankment seismic fragility assessment can be divided into empirical and theoretical methods. Empirical method is based on the field survey of the earthquake zone, and the empirical fragility curves are obtained through the integration of different ground-motion intensities and seismic damage grades [31–33]. Although the results of this method are accurate, its practical applicability is limited due to the following reasons [34–36]:

1. This method requires detailed ground-motion parameter distribution figures of the earthquake zone, but currently the figures are mainly obtained based on the existing attenuation laws combined with the monitoring site record values, their accuracy cannot completely meet the demand.
2. This method requires the damage grade figures of all the structures in the earthquake zone. On the one hand, determining the damage grade is highly subjective and the results are discrete; on the other hand, current damage surveys are mainly sampling surveys that do not cover all the structures in the earthquake zone.
3. This method can reflect the total seismic performances of one type of structure in the earthquake zone, but cannot reflect the specific seismic fragility characteristics of an monomer structure.

It is difficult to apply the empirical method over a wide range, particularly for highways and other linear structures [31, 35–37], therefore, the theoretical method was selected to perform the seismic fragility assessment of the K1025+470 embankment of the Xi'an-Baoji expressway, the main contents were as follows: (1) divide the embankment seismic damage grades, select the embankment seismic damage parameters and establish the relations between the seismic damage grades and seismic damage parameters; (2) establish the finite difference models of the embankment fill-soil foundation system and embankment fill-soil foundation-retaining wall system; (3) select the ground-motion records for IDA and clarify the dynamic response rules of the embankment; (4) determine the exceeding probabilities of different embankment damage grades under different PGAs and generate the fragility curves; (5) verify the influences of the retaining wall on the embankment seismic fragility.

3 Data preparation

Seismic damage grade classification method must be ascertained before assessing the embankment seismic fragility [38, 39]. In HAZUS99, bridges are classified into five states according to seismic performance, namely no damage, slight damage, moderate damage, severe damage and complete destruction [40]. In Japan, seismic damages to bridges, tunnels, slopes and

highways are divided into five grades, namely severe, major, moderate, minor and very minor [41]. Referring to the above studies, embankment seismic damages were divided into five grades, namely basically intact, minor damage, moderate damage, severe damage and destroyed.

Little research has been reported on parameterizing the embankment seismic damages, but by analyzing the seismic damage parameters of other structures, it can be found that the selection of embankment seismic damage parameters should consider the following principles [42–45]:

1. Displacement is the most intuitive reflection of the seismic damages and the definitions of displacement parameters are simple, clear and easy to obtain, therefore, seismic damage parameters are mainly selected based on the displacement failure criterion.
2. Seismic damage parameters are comprehensive reflections of both local and overall seismic damages, they are also quantitative reflections of the degree of use-function reduction, therefore, more than one parameters often be chosen according to the actual situation.

The maximum lateral displacement rate (ε_{max}) and maximum subsidence rate (ζ_{max}) on the surface of the embankment were selected as the seismic damage parameters based on the displacement failure criterion. ε_{max} and ζ_{max} are defined in Eq (1).

$$\varepsilon_{max} = \frac{d_{max}}{D}; \zeta_{max} = \frac{h_{max}}{H} \tag{1}$$

Where d_{max} is the maximum lateral displacement on the surface of the embankment, D is the width of the embankment fill, h_{max} is the maximum subsidence on the surface of the embankment, H is the maximum height of the embankment fill. According to the investigation results of the Wenchuan earthquake, embankments at the epicenter (Yingxiu town) suffered from the most severely damage, i.e. destroyed, and ε_{max} and ζ_{max} reached 1.059% and 1.210% respectively [46–48], therefore, considering ε_{max} = 1.0% and ζ_{max} = 1.2% as the critical values of "severe damage" or "destroyed" is reasonable. Besides, the critical values of ε_{max} and ζ_{max} among other embankment damage grades were further determined based on the equidistant classifying method [20, 38], as summarized in Table 1.

4 IDA of the embankment

4.1 Embankment model

Xi'an-Baoji expressway is located in the Guanzhong plain where some sections are in the form of embankment [49, 50], the K1025+470 embankment was selected as the research object. By referencing on Castaldo et al. [51], a finite difference model of the embankment fill-soil foundation system was established via Flac software. The width of the embankment fill was 24.5m, the right slope was 2.6m high (minimum), the left slope was 6.1m high (maximum) and the

Table 1. Critical values of ε_{max} and ζ_{max}.

Embankment seismic damage grades	Seismic damage parameters	
	ε_{max}/%	ζ_{max}/%
Basically intact	$\varepsilon_{max}<0.2$	$\zeta_{max}<0.2$
Minor damage	$0.2\leq\varepsilon_{max}<0.4$	$0.2\leq\zeta_{max}<0.4$
Moderate damage	$0.4\leq\varepsilon_{max}<0.6$	$0.4\leq\zeta_{max}<0.8$
Severe damage	$0.6\leq\varepsilon_{max}<1.0$	$0.8\leq\zeta_{max}<1.2$
Destroyed	$\varepsilon_{max}\geq1.0$	$\zeta_{max}\geq1.2$

https://doi.org/10.1371/journal.pone.0246407.t001

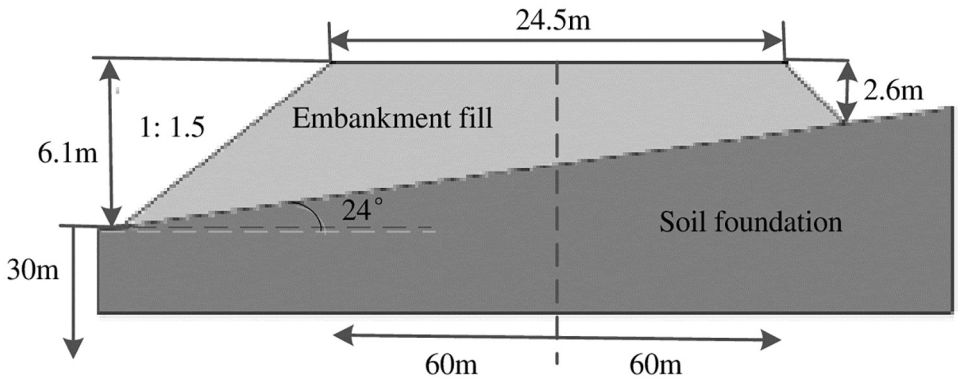

Fig 1. Finite difference model of the embankment fill-soil foundation system.

https://doi.org/10.1371/journal.pone.0246407.g001

slope ratio was 1: 1.5. The dip angle of the soil foundation was 24˚, the thickness was 30m and the width was 120m. Among them, the vehicle loads had been converted to the thickness of the embankment fill according to the elastic layer theory [52], as shown in Fig 1. To verify the influences of the retaining wall on the embankment seismic capabilities, the existence of a RC retaining wall on the left slope of the embankment fill-soil foundation system was assumed, as shown in Fig 2.

An elastoplastic constitutive relation was employed in modeling the embankment fill and soil foundation, while an isotropic elastic constitutive relation was employed in modeling the retaining wall. The Mohr-Coulomb criterion was used as the yield criterion [51], and the mechanical properties of the embankment fill, soil foundation and retaining wall were determined, as shown in Table 2.

Under the actions of the ground-motions, the fundamental motion equation of the embankment fill-soil foundation system and embankment fill-soil foundation-retaining wall system is shown in Eq (2) [53].

$$M\ddot{u} + C\dot{u} + Ku = -MJ\ddot{u}_g \tag{2}$$

Where M refers to the total mass matrix containing the added vehicle mass, C refers to the total damping matrix, K refers to the total stiffness matrix, J refers to the indicator matrix of each seismic component, $\ddot{u}_g$ refers to the action of the ground-motion; $\ddot{u}$, $\dot{u}$ and u refer to the acceleration array, speed array and displacement array of the nodes respectively. The free-

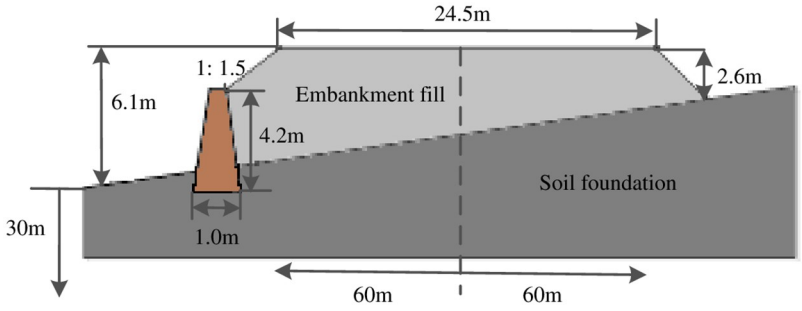

Fig 2. Finite difference model of the embankment fill-soil foundation-retaining wall system.

https://doi.org/10.1371/journal.pone.0246407.g002

Table 2. Mechanical properties of the embankment fill, soil foundation and retaining wall.

Materials	Shear modulus	Density	Elastic modulus	Poisson's ratio
Embankment fill	17.91MPa	1970.00kg/m^3	48.00MPa	0.34
Soil foundation	15.67MPa	1630.00kg/m^3	42.00MPa	0.34
Retaining wall	1282.05MPa	2300.00kg/m^3	3000.00MPa	0.17
Materials	Bulk modulus	Internal friction angle	Cohesive force	
Embankment fill	50.00MPa	33.00°	34.00KPa	
Soil foundation	43.75MPa	28.00°	31.00KPa	
Retaining wall	1515.15MPa	--	--	

https://doi.org/10.1371/journal.pone.0246407.t002

surface boundary was selected as the boundary conditions of the finite difference models, that was, the grids were generated on the model boundaries and the unbalanced forces of the free-surface grids were applied on the main grid boundaries [54]. The Rayleigh damping was adopted as the model damping, which simplified the damping matrix to a linear combination of the mass matrix and stiffness matrix [55]. The seismic fragility assessments were conducted on the embankment fill-soil foundation system and embankment fill-soil foundation-retaining wall system respectively, and the results were then compared [56, 57].

4.2 Determination of the ground-motion records

15 ground-motion records of 8 earthquakes provided by the United States Pacific Earthquake Engineering Research Center (PEER) were selected for IDA [58–60]. The epicentral distances (E_d) of them are in the range of 10.9km to 50.9km, the magnitudes (M_w) are in the range of 5.7 to 7.6 and the original PGA are in the range of 0.094g to 0.968g [61, 62], as shown in Table 3.

Due to the limited space, the acceleration time history curves of the No.1-No.3 ground-motion records are listed in Fig 3.

In order to get the dynamic response characteristics of the embankment fill-soil foundation system and embankment fill-soil foundation-retaining wall system under different ground-motion intensities, the selected ground-motion records need to be adjusted to higher or lower intensity levels, that is, the amplitude modulation of ground-motion records. PGA of each ground-motion record was adjusted to 0.2g, 0.4g, 0.6g, 0.8g, 1.0g and 1.2g respectively, and obtained 90 ground- motion records [63, 64].

4.3 Dynamic response analysis

The 90 ground-motion records were input to the established models of the embankment fill-soil foundation system and embankment fill-soil foundation-retaining wall system for 180

Table 3. Seismic ground-motion records.

No.	Earthquake	E_d	M_w	Original PGA	No.	Earthquake	E_d	M_w	Original PGA
1	Kobe_Japan	49.9km	6.9	0.094g	9	Cape Mendocino-2	18.5km	7.1	0.385g
2	Landers	50.9km	7.3	0.117g	10	Chalfont Valley-3	11.7km	6.0	0.447g
3	Bishop (Rnd Val)	19.0km	5.7	0.128g	11	Cape Mendocino-3	13.5km	7.1	0.591g
4	San Simeon_CA	38.0km	6.5	0.132g	12	Chi-Chi, Taiwan-1	26.0km	7.6	0.639g
5	Duzce_Turkey	34.3km	7.1	0.138g	13	Chi-Chi, Taiwan-2	18.8km	7.6	0.724g
6	Chalfont Valley-1	20.0km	6.0	0.143g	14	Chi-Chi, Taiwan-3	13.4km	7.6	0.821g
7	Cape Mendocino-1	33.8km	7.1	0.229g	15	Chi-Chi, Taiwan-4	10.9km	7.6	0.968g
8	Chalfont Valley-2	16.2km	6.0	0.248g					

https://doi.org/10.1371/journal.pone.0246407.t003

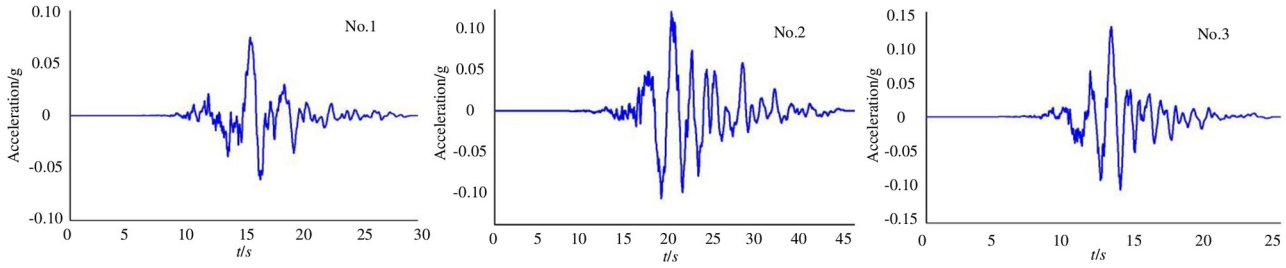

Fig 3. Acceleration time history curves of the No.1-No.3 ground-motion records.

https://doi.org/10.1371/journal.pone.0246407.g003

dynamic response analysis. A total of 50 monitoring points were set up at every 0.5m on the surface of the embankment. The lateral displacement d and subsidence h at different monitoring points and different times as well as their mean values were recorded, and ε_{max}, ζ_{max} and their mean values were calculated as shown in Tables 4 and 5.

Fig 4 illustrates the time histories of the mean values of ε_{max} and ζ_{max} on the monitoring point No.1 (left edge of the surface) of the embankment fill-soil foundation system and embankment fill-soil foundation-retaining wall system when PGA = 1.2g. It is evident from Fig 4 that the retaining wall reduces ε_{max} and ζ_{max} by 13.02% and 10.63% respectively.

4.4 IDA results

According to Karthik et al. [65], Alielahi and Moghadam [66] and Pang [67], ε_{max} and PGA follow the exponential relation, as shown in Eq (3).

$$\ln\ \varepsilon_{max} = \ln\ a_1 + b_1\ \ln\ \mathrm{PGA} \tag{3}$$

Where a_1 and b_1 are estimated parameters. Similarly, ζ_{max} and PGA follow the relation shown in Eq (4).

$$\ln\ \zeta_{max} = \ln\ a_2 + b_2\ \ln\ \mathrm{PGA} \tag{4}$$

Table 4. Dynamic response analysis results of the embankment fill-soil foundation system.

Serial number of the ground- motion records	0.2g		0.4g		0.6g		0.8g		1.0g		1.2g	
	ε_{max}/%	ζ_{max}/%	ε_{max}/%	ζ_{max}/%	ε_{max}/%	ζ_{max}/%	ε_{max}/%	ζ_{max}/%	ε_{max}/%	ζ_{max}/%	ε_{max}/%	ζ_{max}/%
1	0.1579	0.1812	0.4239	0.4876	0.5219	0.6389	0.8126	0.9937	1.3648	1.1854	1.4047	1.7159
2	0.2203	0.1438	0.3568	0.4471	0.5868	0.6977	0.7534	0.8543	1.2694	1.3148	1.5843	1.5342
3	0.1629	0.1398	0.3459	0.5128	0.5098	0.6018	0.8637	0.8875	1.1458	1.2991	1.4143	1.6487
4	0.2164	0.1716	0.4103	0.4095	0.5717	0.6844	0.8225	0.9109	1.3694	1.2675	1.5436	1.5846
5	0.1854	0.1379	0.3846	0.4167	0.5529	0.5079	0.7201	0.8456	1.1129	1.2834	1.5756	1.5241
6	0.1788	0.1812	0.4572	0.4891	0.5324	0.6047	0.7968	1.0077	1.2287	1.2037	1.5149	1.6008
7	0.1763	0.1251	0.3521	0.4359	0.6487	0.6387	0.7816	0.9768	1.1567	1.3651	1.5884	1.6017
8	0.1944	0.1723	0.3854	0.4765	0.5249	0.6916	0.8055	0.8391	1.3042	1.2513	1.4371	1.5418
9	0.1724	0.1454	0.4086	0.4123	0.6273	0.5721	0.7484	0.8746	1.1964	1.2789	1.6294	1.7309
10	0.1605	0.1948	0.3695	0.4896	0.5951	0.5948	0.7338	0.9427	1.2523	1.3811	1.5055	1.5281
11	0.1864	0.1335	0.4187	0.4312	0.5437	0.6989	0.8219	0.9009	1.0894	1.2846	1.5156	1.6807
12	0.2039	0.1861	0.4531	0.5195	0.5892	0.6251	0.7218	0.8248	1.1746	1.3718	1.5786	1.5438
13	0.1686	0.1565	0.4015	0.4047	0.5684	0.6984	0.6146	0.9986	1.1989	1.3064	1.4572	1.7158
14	0.1701	0.1779	0.4365	0.5464	0.5145	0.7478	0.7343	1.1001	1.3568	1.4049	1.3926	1.7872
15	0.1912	0.1248	0.3486	0.3751	0.6367	0.5495	0.7965	0.8064	1.1057	1.1285	1.6357	1.4597
Mean values	0.1830	0.1581	0.3968	0.4569	0.5683	0.6368	0.7685	0.9176	1.2217	1.2884	1.5185	1.6132

https://doi.org/10.1371/journal.pone.0246407.t004

Table 5. Dynamic response analysis results of the embankment fill-soil foundation-retaining wall system.

Serial number of the ground- motion records	0.2g		0.4g		0.6g		0.8g		1.0g		1.2g	
	ε_{max}/%	ζ_{max}/%	ε_{max}/%	ζ_{max}/%	ε_{max}/%	ζ_{max}/%	ε_{max}/%	ζ_{max}/%	ε_{max}/%	ζ_{max}/%	ε_{max}/%	ζ_{max}/%
1	0.1192	0.0918	0.2771	0.2404	0.5276	0.5723	0.7542	0.8132	0.9679	1.1926	1.0257	1.1859
2	0.1097	0.1397	0.3281	0.3235	0.4151	0.4475	0.6343	0.6908	0.9287	1.0737	1.2459	1.2062
3	0.1412	0.1146	0.2932	0.2862	0.4292	0.5314	0.6537	0.7345	0.8782	0.9822	1.1732	1.2048
4	0.1266	0.1251	0.2906	0.2533	0.5387	0.4097	0.6443	0.6825	0.9103	1.0246	1.0362	1.3659
5	0.0958	0.0995	0.3393	0.2962	0.4262	0.5681	0.7016	0.7936	0.8583	1.0251	1.0842	1.4351
6	0.1481	0.1182	0.2806	0.2777	0.4384	0.4561	0.6732	0.7233	0.9437	0.8681	1.2235	1.2392
7	0.1026	0.1004	0.2414	0.2546	0.5007	0.5217	0.6497	0.7951	0.8831	1.0147	1.0267	1.4732
8	0.1408	0.1332	0.2995	0.2892	0.4116	0.5362	0.7316	0.8063	0.9059	0.9462	1.3006	1.1687
9	0.1129	0.1287	0.3056	0.2685	0.4282	0.4417	0.7096	0.7092	0.9635	1.0726	1.1876	1.2054
10	0.1487	0.1263	0.2414	0.2751	0.4997	0.4393	0.6472	0.7846	0.8847	1.0055	1.1046	1.3296
11	0.1243	0.1035	0.2298	0.2994	0.4258	0.5406	0.7351	0.7156	0.8462	1.1233	0.9258	1.4387
12	0.1074	0.0986	0.3037	0.2424	0.5081	0.5571	0.6943	0.6973	0.9517	1.0687	1.2533	1.2057
13	0.1286	0.0909	0.2834	0.2615	0.4679	0.4236	0.6625	0.8481	0.9028	1.1254	1.0932	1.3288
14	0.0919	0.1184	0.2587	0.2796	0.4136	0.5672	0.6234	0.8762	0.9716	0.9239	0.9953	1.4841
15	0.1489	0.1365	0.3316	0.2681	0.5517	0.4153	0.7768	0.6672	0.8346	0.9013	1.2782	1.1561
Mean values	0.1231	0.1150	0.2869	0.2744	0.4655	0.4952	0.6861	0.7558	0.9087	1.0232	1.1303	1.2952

https://doi.org/10.1371/journal.pone.0246407.t005

According to the dynamic response analysis results, regressions on a_1, b_1, a_2 and b_2 were performed and Fig 5 was obtained.

The relations between ε_{max}, ζ_{max} and PGA of the embankment fill-soil foundation system are shown in Eqs (5) and (6), and the relations between ε_{max}, ζ_{max} and PGA of the embankment fill-soil foundation-retaining wall system are shown in Eqs (7) and (8).

$$\varepsilon_{max} = 1.1317\mathrm{PGA}^{1.1618}. \tag{5}$$

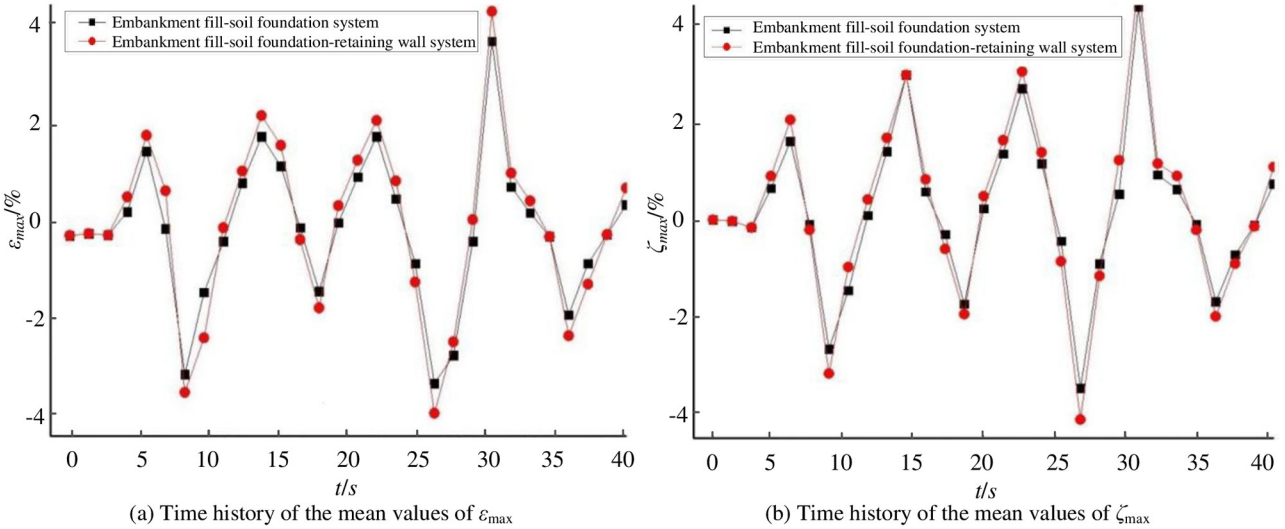

(a) Time history of the mean values of ε_{max}

(b) Time history of the mean values of ζ_{max}

Fig 4. Time histories of the mean values of ε_{max} and ζ_{max} (positive values represent subsidence, negative values represent tilt).

https://doi.org/10.1371/journal.pone.0246407.g004

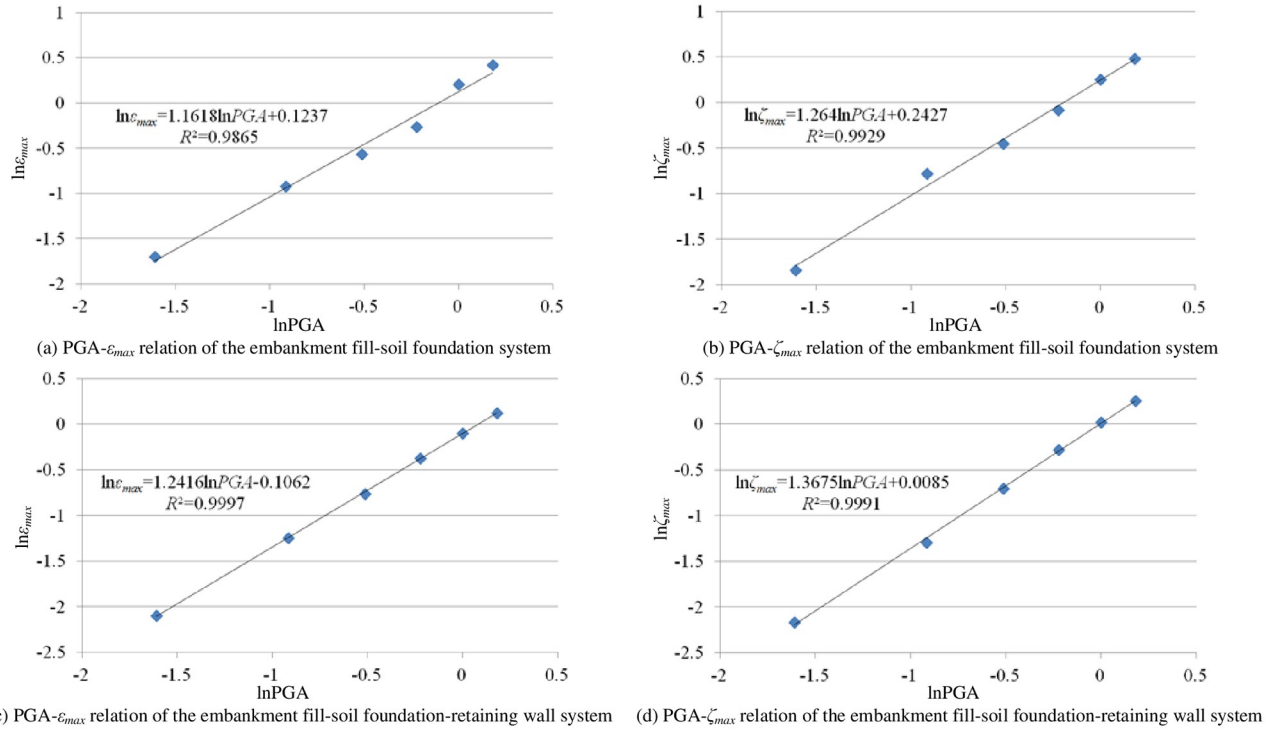

Fig 5. IDA results.

https://doi.org/10.1371/journal.pone.0246407.g005

$$\zeta_{max} = 1.2747\mathrm{PGA}^{1.264} \tag{6}$$

$$\varepsilon_{max} = 0.8992\mathrm{PGA}^{1.2416}. \tag{7}$$

$$\zeta_{max} = 1.0085\mathrm{PGA}^{1.3675}. \tag{8}$$

5 Embankment seismic fragility assessment results

5.1 Seismic fragility curves

Eqs (5)–(8) were substituted into the classical calculation equation of the seismic fragility to obtain Eqs (9)–(12), which Eqs (9) and (10) were the seismic fragility equations of the embankment fill-soil foundation system considering ε_{max} and ζ_{max} as the seismic damage parameters respectively, and Eqs (11) and (12) were the seismic fragility equations of the embankment fill-soil foundation-retaining wall system considering ε_{max} and ζ_{max} as the seismic damage parameters respectively [68–70].

$$P_j = \Phi(2 \cdot \ln\ (1.1317\mathrm{PGA}^{1.1618}/S_j)) \tag{9}$$

$$P_j = \Phi(2 \cdot \ln\ (1.2747\mathrm{PGA}^{1.264}/S_j)) \tag{10}$$

$$P_j = \Phi(2 \cdot \ln\ (0.8992\mathrm{PGA}^{1.2416}/S_j)) \tag{11}$$

$$P_j = \Phi(2 \cdot \ln\ (1.0085\mathrm{PGA}^{1.3675}/S_j)) \tag{12}$$

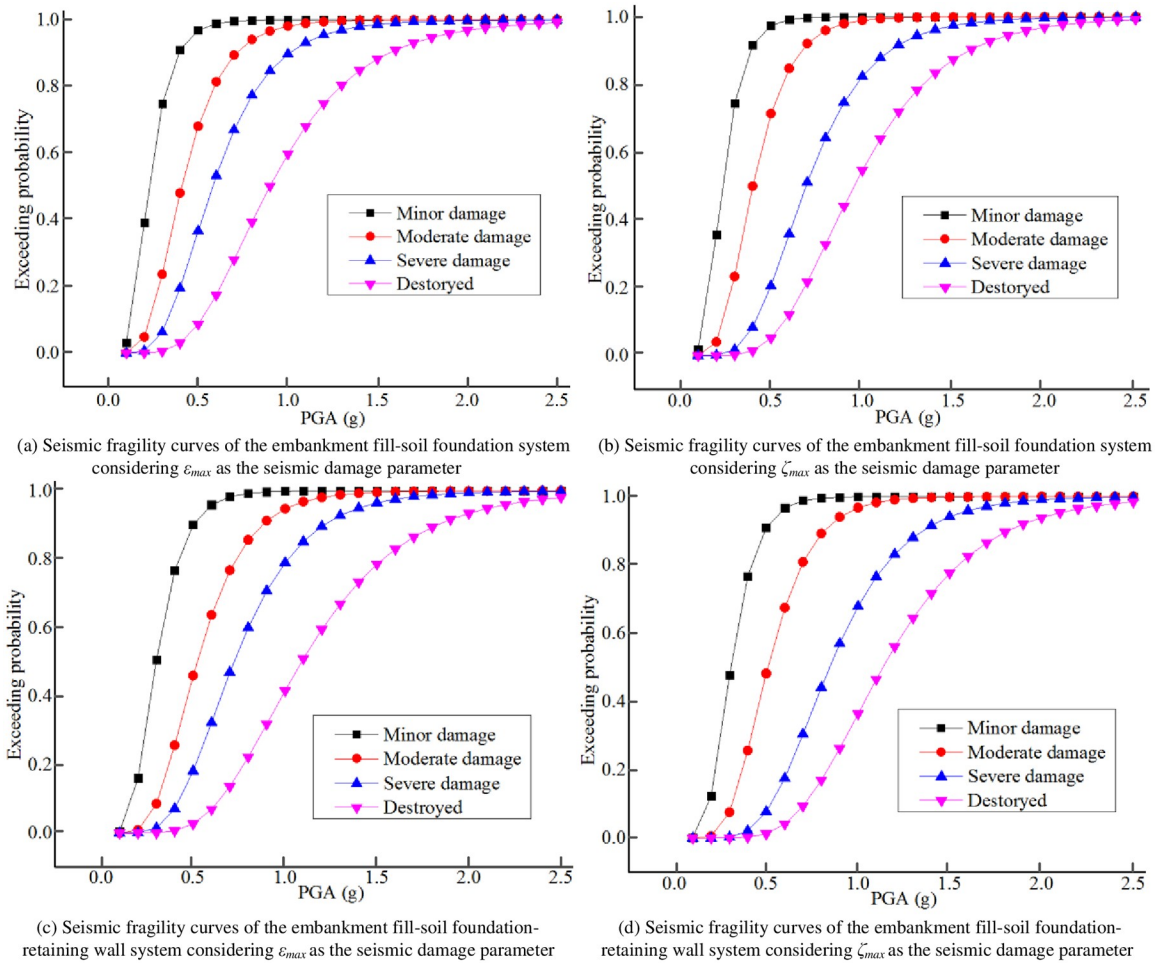

(a) Seismic fragility curves of the embankment fill-soil foundation system considering ε_{max} as the seismic damage parameter

(b) Seismic fragility curves of the embankment fill-soil foundation system considering ζ_{max} as the seismic damage parameter

(c) Seismic fragility curves of the embankment fill-soil foundation-retaining wall system considering ε_{max} as the seismic damage parameter

(d) Seismic fragility curves of the embankment fill-soil foundation-retaining wall system considering ζ_{max} as the seismic damage parameter

Fig 6. Seismic fragility curves.

https://doi.org/10.1371/journal.pone.0246407.g006

Where P_j refers to the exceeding probability of the embankment seismic damage grade j, and $j = 1$ represents basically intact, $j = 2$ represents minor damage, $j = 3$ represents moderate damage, $j = 4$ represents severe damage, $j = 5$ represents destroyed; S_j refers to the structural performance level shown in Table 1, namely $S_2 = 0.20$, $S_3 = 0.40$, $S_4 = 0.60$, $S_5 = 1.00$ when considering ε_{max} as the seismic damage parameter, and $S_2 = 0.20$, $S_3 = 0.40$, $S_4 = 0.80$, $S_5 = 1.20$ when considering ε_{max} as the seismic damage parameter [71–73]. The embankment seismic fragility curves were generated according to Eqs (9)–(12), as shown in Fig 6.

5.2 Discussion

According to Fig 6, PGAs corresponding to each seismic damage grade with exceeding probabilities of 30%, 50% and 80% of the embankment fill-soil foundation system and embankment fill-soil foundation-retaining wall system were obtained, as summarized in Table 6.

It is evident from Table 6 that although the coupling mechanism and mechanical process of the embankment fill, soil foundation and retaining wall under the earthquake actions are unclear, the embankment fill-soil foundation- retaining wall system always suffers from less damages than those of the embankment fill-soil foundation system. For example, for exceeding

Table 6. PGAs corresponding to each seismic damage grade with different exceeding probabilities.

Exceeding probabilities	Research objects	PGAs			
		Minor damage	Moderate damage	Severe damage	Destroyed
30%	Embankment fill-soil foundation system	0.1868g, 0.1947g	0.3393g, 0.3370g	0.4809g, 0.5831g	0.7465g, 0.8036g
	Embankment fill-soil foundation-retaining wall system	0.2504g, 0.2616g	0.4377g, 0.4343g	0.6067g, 0.7209g	0.9155g, 0.9697g
50%	Embankment fill-soil foundation system	0.2250g, 0.2310g	0.4085g, 0.3997g	0.5792g, 0.6917g	0.8990g, 0.9533g
	Embankment fill-soil foundation-retaining wall system	0.2980g, 0.3063g	0.5208g, 0.5085g	0.7219g, 0.8442g	1.0893g, 1.1356g
80%	Embankment fill-soil foundation system	0.3031g, 0.3039g	0.5505g, 0.5258g	0.7804g, 0.9099g	1.2114g, 1.2540g
	Embankment fill-soil foundation-retaining wall system	0.3939g, 0.3947g	0.6884g, 0.6552g	0.9543g, 1.0877g	1.4400g, 1.4630g

Note: the first data in each blank is the PGA when considering ε_{max} as the seismic damage parameter, while the second data is the PGA when considering ζ_{max} as the seismic damage parameter.

https://doi.org/10.1371/journal.pone.0246407.t006

probabilities of 30%, 50% and 80%, the PGAs corresponding to the embankment fill-soil foundation-retaining wall system are 20.56%, 20.12% and 17.75% higher than those of the embankment fill-soil foundation system respectively when "destroyed" occurred, therefore, more serious seismic damages are less likely to happen to the embankment fill-soil foundation-retaining wall system. Similarly, the probabilities of each seismic damage grade of the embankment fill-soil foundation system and embankment fill-soil foundation-retaining wall system corresponding to different PGAs were calculated, as summarized in Table 7.

Table 7. Probabilities of each seismic damage grade corresponding to different PGAs.

Research objects	Seismic damage parameters	Seismic damage grades	Exceeding probabilities of each seismic damage grade corresponding to different PGAs											
			0.1g	0.2g	0.3g	0.4g	0.5g	0.6g	0.7g	0.8g	0.9g	1.0g	1.1g	1.2g
Embankment fill-soil foundation system	ε_{max}	Basically intact	1.0000	1.0000	1.0000	1.0000	1.0000	1.0000	1.0000	1.0000	1.0000	1.0000	1.0000	1.0000
		Minor damage	0.0298	0.3923	0.7482	0.9094	0.9683	0.9887	0.9958	0.9984	0.9994	0.9997	0.9999	0.9999
		Moderate damage	0.0005	0.0485	0.2365	0.4804	0.6806	0.8141	0.8946	0.9408	0.9668	0.9812	0.9893	0.9939
		Severe damage	0.0000	0.0067	0.0632	0.1949	0.3664	0.5327	0.6701	0.7736	0.8471	0.8978	0.9320	0.9547
		Destroyed	0.0000	0.0002	0.0054	0.0299	0.0864	0.1737	0.2805	0.3932	0.5010	0.5977	0.6804	0.7489
	ζ_{max}	Basically intact	1.0000	1.0000	1.0000	1.0000	1.0000	1.0000	1.0000	1.0000	1.0000	1.0000	1.0000	1.0000
		Minor damage	0.0171	0.3578	0.7456	0.9174	0.9745	0.9921	0.9975	0.9992	0.9994	0.9996	0.9998	0.9999
		Moderate damage	0.0002	0.0400	0.2340	0.5006	0.7142	0.8477	0.9217	0.9603	0.9799	0.9898	0.9948	0.9973
		Severe damage	0.0000	0.0009	0.0173	0.0831	0.2059	0.3596	0.5120	0.6434	0.7471	0.8242	0.8795	0.9181
		Destroyed	0.0000	0.0000	0.0017	0.0141	0.0514	0.1209	0.2174	0.3288	0.4421	0.5481	0.6412	0.7196
Embankment fill-soil foundation-retaining wall system	ε_{max}	Basically intact	1.0000	1.0000	1.0000	1.0000	1.0000	1.0000	1.0000	1.0000	1.0000	1.0000	1.0000	1.0000
		Minor damage	0.0036	0.1610	0.5067	0.7676	0.9006	0.9589	0.9830	0.9929	0.9970	0.9987	0.9994	0.9997
		Moderate damage	0.0000	0.0087	0.0854	0.2562	0.4597	0.6374	0.7686	0.8568	0.9128	0.9474	0.9683	0.9809
		Severe damage	0.0000	0.0007	0.0146	0.0713	0.1809	0.3230	0.4695	0.6007	0.7080	0.7908	0.8522	0.8965
		Destroyed	0.0000	0.0000	0.0007	0.0064	0.0266	0.0693	0.1361	0.2217	0.3177	0.4159	0.5096	0.5949
	ζ_{max}	Basically intact	1.0000	1.0000	1.0000	1.0000	1.0000	1.0000	1.0000	1.0000	1.0000	1.0000	1.0000	1.0000
		Minor damage	0.0011	0.1219	0.4772	0.7672	0.9099	0.9670	0.9881	0.9957	0.9984	0.9994	0.9998	0.9999
		Moderate damage	0.0000	0.0054	0.0745	0.2557	0.4816	0.6745	0.8089	0.8924	0.9408	0.9678	0.9826	0.9906
		Severe damage	0.0000	0.0000	0.0023	0.0205	0.0760	0.1752	0.3042	0.4415	0.5695	0.6784	0.7654	0.8319
		Destroyed	0.0000	0.0000	0.0001	0.0022	0.0124	0.0405	0.0929	0.1690	0.2624	0.3640	0.4653	0.5600

https://doi.org/10.1371/journal.pone.0246407.t007

It is evident from Table 7 that regardless of which seismic damage parameter is considered or the presence or absence of the retaining wall, larger PGAs always correspond to higher probabilities of each seismic damage grade. For example, when PGA = 1.2g, the probabilities of the embankment fill-soil foundation system being "destroyed" are 11.12% and 18.46% respectively higher on average than those when PGA = 1.1g. On the other hand, the seismic damages to the embankment fill-soil foundation-retaining wall system are always lower than those of the embankment fill-soil foundation system under the same PGA actions. For example, when PGA = 1.2g, the probability of the embankment fill-soil foundation-retaining wall system being "destroyed" is 27.15% lower than that of the embankment fill-soil foundation system, thus, the retaining wall can decrease the embankment seismic fragility significantly.

6 Conclusions

1. Embankment seismic damages were divided into 5 grades, the maximum lateral displacement rate (ε_{max}) and maximum subsidence rate (ζ_{max}) on the surface of the embankment were selected as the seismic damage parameters. The K1025+470 embankment of the Xi'an-Baoji expressway was studied, the structure forms of the embankment fill-soil foundation system and embankment fill-soil foundation-retaining wall system were determined and the finite difference models were established via Flac software. The ground-motion records for IDA were selected and the dynamic response analysis were conducted. The PSDA was used to deal with the IDA results and generated the seismic fragility curves, the influences of the RC retaining wall on the embankment seismic fragility were further determined.
2. Regardless of which seismic damage parameter was considered or the presence or absence of the retaining wall, larger PGAs always correspond to higher probabilities of each seismic damage grade. Under the same PGA actions, the seismic damages to the embankment fill-soil foundation-retaining wall system are always lower than those of the embankment fill-soil foundation system, thus, the retaining wall can decrease the embankment seismic fragility significantly.
3. Although the embankment seismic fragility assessment was studied in this paper, the following problems still remained. First, while ε_{max} and ζ_{max} have feasibilities as the embankment seismic damage parameters, they still could not fully reflect the embankment seismic damage characteristics, selecting more reasonable parameters is yet to be studied. Second, there are multiple factors influencing the embankment seismic fragility, the influences of the retaining wall were quantitatively studied, the influences of other factors are yet to be studied. Third, design parameters of the embankment, such as the dip angle of the soil foundation may play an important role in the embankment seismic performance according to existing studies, therefore, sensitive analysis about dip angle should be performed in subsequence studies.

Supporting information

S1 Data.
(XLSX)

Acknowledgments

The authors of this article would like to thank Haoran Li for his advice on writing this article.

Author Contributions

Conceptualization: Fa Che, Zhinan Hu, Dong Liu.

Data curation: Chao Yin.

Formal analysis: Xingkui Zhao.

Funding acquisition: Fa Che, Chao Yin, Dong Liu.

Investigation: Zhinan Hu, Lu Sheng.

Methodology: Fa Che, Chao Yin.

Project administration: Chao Yin, Xingkui Zhao.

Resources: Zhinan Hu, Lu Sheng.

Software: Fa Che, Dong Liu.

Supervision: Chao Yin, Xingkui Zhao.

Validation: Fa Che, Zhinan Hu, Lu Sheng.

Visualization: Dong Liu.

Writing – original draft: Fa Che, Chao Yin, Xingkui Zhao.

Writing – review & editing: Chao Yin.

References

1. Zhao XQ, Wang FD, Verheyden S, Liu JZ, Zhang G (2020) Earthquake-related speleothem damages: observations from the 2008 Mw 7.9 Wenchuan, China. Geomorphology 358:107130.
2. Xu CX, Deng J, Peng S, Li CY (2018) Seismic fragility analysis of steel reinforced concrete frame structures based on different engineering demand parameters. Journal of Building Engineering 20:736–749.
3. Enomoto T, Sasaki T (2018) Seismic behavior of reinforced embankments in dynamic centrifuge model tests. Soils & Foundations 58(1):212–227.
4. Modoni G, Albano M, Salvatore E, Koseki J (2018) Effects of compaction on the seismic performance of embankments built with gravel. Soil Dynamics and Earthquake Engineering 106:231–242.
5. Yang SC, Gao YF, Leshchinsky B, Cui K, Zhang F (2020) Internal stability analysis of reinforced convex highway embankments considering seismic loading. Geotextiles and Geomembranes 48(3):221–229.
6. Yoshikawa T, Noda T, Kodaka T, Takaine T (2016) Analysis of the effect of groundwater level on the seismic behavior of an unsaturated embankment on clayey ground. Soil Dynamics and Earthquake Engineering 85:217–230.
7. Dang CT, Le TP, Ray P (2017) A novel method based on maximum likelihood estimation for the construction of seismic fragility curves using numerical simulations. Comptes Rendus Mécanique 345 (10):678–689.
8. Xie YZ, DesRoches R (2019) Sensitivity of seismic demands and fragility estimates of a typical California highway bridge to uncertainties in its soil-structure interaction modeling. Engineering Structures 189:605–617.
9. Adafer S, Bensaibi M (2017) Seismic vulnerability classification of roads. Energy Procedia 139:624–630.
10. Billah AM, Todorov B (2019) Effects of subfreezing temperature on the seismic response of lead rubber bearing isolated bridge. Soil Dynamics and Earthquake Engineering 126:105814.
11. Yin C (2020) Hazard evaluation and regionalization of highway flood disasters in China. Natural Hazards 200:535–550.
12. Zhang LW, Lu ZH, Chen C (2020) Seismic fragility analysis of bridge piers using methods of moment. Soil Dynamics and Earthquake Engineering 134:106150.
13. Xu JG, Wu G, Feng DC, Cotsovos DM, Lu Y (2020) Seismic fragility analysis of shear-critical concrete columns considering corrosion induced deterioration effects. Soil Dynamics and Earthquake Engineering 134:106165.

14. Xiang NL, Chen X, Alam MS (2020) Probabilistic seismic fragility and loss analysis of concrete bridge piers with superelastic shape memory alloy-steel coupled reinforcing bars. Engineering Structures 207:110229.

15. Melani A., Khare RK, Dhakal RP, Mander JB (2016) Seismic risk assessment of low-rise RC frame structure. Structures 5:13–22.

16. Wang JT, Zhang MX, Jin AY, Zhang CH (2018) Seismic fragility of arch dams based on damage analysis. Soil Dynamics & Earthquake Engineering 109:58–68.

17. Ko YY, Yang HH (2019) Deriving seismic fragility curves for sheet-pile wharves using finite element analysis. Soil Dynamics and Earthquake Engineering 123:265–277.

18. Liu KH, Yan JC, Alam MS, Zou CY (2019) Seismic fragility analysis of deteriorating recycled aggregate concrete bridge columns subjected to freeze-thaw cycles. Engineering Structures 187:1–15.

19. Yoon S, Lee DH, Jung HJ (2019) Seismic fragility analysis of a buried pipeline structure considering uncertainty of soil parameters. International Journal of Pressure Vessels and Piping 175:103932.

20. Bao X, Zhang MH, Zhai CH (2019) Fragility analysis of a containment structure under far-fault and near-fault seismic sequences considering post-mainshock damage states. Engineering Structures 198:109511.

21. Chen Z, Yang P, Liu H, Zhang W, Wu C (2019) Characteristics analysis of granular landslide using shaking table model test. Soil Dynamics and Earthquake Engineering 126:105761.

22. Pan HY, Tian L, Fu X, Li HN (2020) Sensitivities of the seismic response and fragility estimate of a transmission tower to structural and ground motion uncertainties. Journal of Constructional Steel Research 167:105941.

23. Sainct R, Feau C, Martinez JM, Garnier J (2020) Efficient methodology for seismic fragility curves estimation by active learning on Support Vector Machines. Structural Safety 86:101972.

24. Sarno LD, Pugliese F (2020) Seismic fragility of existing RC buildings with corroded bars under earthquake sequences. Soil Dynamics and Earthquake Engineering 134:106169.

25. Liang H, Tu J, Guo SS, Liao JX, Li DY, Peng SQ (2020) Seismic fragility analysis of a High Arch Dam-Foundation System based on seismic instability failure mode. Soil Dynamics and Earthquake Engineering 130:105981.

26. Kumar P, Samanta A (2020) Seismic fragility assessment of existing reinforced concrete buildings in Patna, India. Structures 27:54–69.

27. Ciano M, Gioffrè M, Grigoriu M (2020) The role of intensity measures on the accuracy of seismic fragilities. Probabilistic Engineering Mechanics 60:103041.

28. Ebrahimi E, Abdollahzadeh G, Jahani E (2020) Developing the seismic fragility analysis with fuzzy random variables using Mouth Brooding Fish algorithm. Applied Soft Computing 91:106190.

29. Ding XM, Feng L, Wang CL, Chen ZX, Han L (2020) Shaking table tests of the seismic response of a utility tunnel with a joint connection. Soil Dynamics and Earthquake Engineering 133:106133.

30. Stefanidou SP, Sextos AG, Kotsoglou AN, Lesgidis N, Kappos AJ (2017) Soil-structure interaction effects in analysis of seismic fragility of bridges using an intensity-based ground motion selection procedure. Engineering Structures 151:366–380.

31. Yazgan U (2015) Empirical seismic fragility assessment with explicit modeling of spatial ground motion variability. Engineering Structures 100:479–489

32. Hofer L, Zampieri P, Zanini MA, Faleschini F, Pellegrino C (2018) Seismic damage survey and empirical fragility curves for churches after the August 24, 2016 Central Italy earthquake. Soil Dynamics and Earthquake Engineering 111:98–109

33. Zhong ZL, Shen YY, Zhao M, Li LY, Du XL, Hao H (2020) Seismic fragility assessment of the Daikai subway station in layered soil. Soil Dynamics and Earthquake Engineering 132:106044.

34. Straub D, Kiureghian AD (2008) Improved seismic fragility modeling from empirical data. Structural Safety 30(4):320–336.

35. Lorenzo H, Paolo Z, Angelo ZM, Flora F, Carlo P (2018) Seismic damage survey and empirical fragility curves for churches after the August 24, 2016 central Italy earthquake. Soil Dynamics and Earthquake Engineering 111:98–109.

36. Foytong P, Ornthammarath T (2020) Empirical seismic fragility functions based on field survey data after the 5 May 2014 Mae Lao (Northern Thailand) earthquake. International Journal of Disaster Risk Reduction 42:101344.

37. Andreotti G, Lai CG (2019) Use of fragility curves to assess the seismic vulnerability in the risk analysis of mountain tunnels. Tunneling and Underground Space Technology 91:103008.

38. Xu CX, Peng S, Liu XQ, Wang CF, Xu QQ (2020) Analysis of the seismic behavior of CFRP-strengthened seismic-damaged composite steel-concrete frame joints. Journal of Building Engineering 28:101057.

39. Morfidis K, Kostinakis K (2019) Comparative evaluation of MFP and RBF neural networks' ability for instant estimation of r/c buildings' seismic damage level. Engineering Structures 197:109436.

40. Silva V, Crowley H, Varum H, Rui P (2015) Seismic risk assessment for mainland Portugal. Bulletin of Earthquake Engineering 13:429–457.

41. Tsompanakis Y, Lagaros ND, Psarropoulos PN, Georgopoulos EC (2009) Simulating the seismic response of embankments via artificial neural networks. Advances in Engineering Software 40(8):640–651.

42. Yang XL (2007) Seismic displacement of rock slopes with nonlinear Hoek-Brown failure criterion. International Journal of Rock Mechanics and Mining Sciences 44(6):948–953.

43. Zhao LH, Cheng X, Li L, Chen JQ, Zhang YB (2017) Seismic displacement along a log-spiral failure surface with crack using rock Hoek-Brown failure criterion. Soil Dynamics and Earthquake Engineering 99:74–85.

44. Hashemi A, Quenneville P (2020) Seismic performance of timber structures using rocking walls with low damage hold-down connectors. Structures 27:274–284.

45. Guo X, He Z, Xu JJ (2020) Identification of incremental seismic damage development in RC structures excited with sequence-type ground motions. Structures 24:464–476.

46. Zhang JM, Yang ZY, Gao XZ, Zhang JH (2015) Geotechnical aspects and seismic damage of the 156-m-high Zipingpu concrete-faced rockfill dam following the Ms8.0 Wenchuan earthquake. Soil Dynamics and Earthquake Engineering 76:145–156.

47. Lin P, Huang B, Li QB, Wang RK (2015) Hazard and seismic reinforcement analysis for typical large dams following the Wenchuan earthquake. Engineering Geology 194:86–97.

48. Han B, Zdravkovic L, Kontoe S, Taborda DMG (2016) Numerical investigation of the response of the Yele rockfill dam during the 2008 Wenchuan earthquake. Soil Dynamics and Earthquake Engineering 88:124–142.

49. Zhang XJ, Gao ZL, Li J, Tian HW (2012) Variation of soil nutrients and mode of α diversity of plant community on the embankment slope of highways in Guanzhong Plain. Research of Soil and Water Conservation 19(6):157–162. (in Chinese)

50. Yin C, Liu FF, Zhang JL (2017) Seismic hazard assessment of Xi'an-Baoji expressway. Earthquake Engineering and Engineering Dynamics 37(2): 181–188. (in Chinese)

51. Castaldo P, Gino D, Mancini G (2019) Safety formats for non-linear finite element analysis of reinforced concrete structures: discussion, comparison and proposals. Engineering Structures 193:136–153.

52. Mercer B, Mandadapu KK, Papadopoulos P (2016) Homogenization of high-frequency wave propagation in linearly elastic layered media using a continuum Irving-Kirkwood theory. International Journal of Solids and Structures 96:162–172.

53. Castaldo P, De Iuliis M (2014) Effects of deep excavation on seismic vulnerability of existing reinforced concrete framed structures. Soil Dynamics and Earthquake Engineering 64:102–112.

54. Oishi CM, Thompson RL, Martins FP (2016) Transient motions of elasto-viscoplastic thixotropic materials subjected to an imposed stress field and to stress-based free-surface boundary conditions. International Journal of Engineering Science 109165–201.

55. Yılmaz İ, Arslan E, Kızıltaş EC, Çavdar K (2020) Development of a prediction method of Rayleigh damping coefficients for free layer damping coatings through machine learning algorithms. International Journal of Mechanical Sciences 166:105237.

56. Lin CG, Huang MS, Nadim F, Liu ZQ (2020) Embankment responses to shield tunneling considering soil-structure interaction: case studies in Hangzhou soft ground. Tunnelling and Underground Space Technology 96:103230.

57. Yang SC, Gao YF, Leshchinsky B, Cui K, Zhang F (2020) Internal stability analysis of reinforced convex highway embankments considering seismic loading. Geotextiles and Geomembranes 48(3):221–229.

58. Zheng Z, Hoogenboom G, Cai HJ, Wang ZK (2020) Winter wheat production on the Guanzhong Plain of Northwest China under projected future climate with SimCLIM. Agricultural Water Management 238:106233.

59. Abyani M, Bahaari MR, Zarrin M, Nasseri M (2019) Effects of sample size of ground motions on seismic fragility analysis of offshore jacket platforms using Genetic Algorithm. Ocean Engineering 189:106326.

60. Su L, Wan HP, Dong Y, Frangopol DM, Ling XZ (2019) Seismic fragility assessment of large-scale pile-supported wharf structures considering soil-pile interaction. Engineering Structures 186:270–281.

61. Sengupta P, Li B (2016) Seismic fragility assessment of lightly reinforced concrete structural walls. Journal of Earthquake Engineering 20:809–840.

62. Shimbo T (2017) Development and application of a dynamic XFEM for the seismic residual displacement analysis of an embankment. Soils and Foundations 57(3):357–370.

63. Zhen C, Wei-Chau X, Pandey MD, Shun-Hao N (2018) Determining seismic fragility of structures and components in nuclear power plants using multiple ground motion parameters-Part one: methodology. Nuclear Engineering and Design 335:195–201.

64. Pang R, Xu B, Kong XJ, Zou DG (2018) Seismic fragility for high CFRDs based on deformation and damage index through incremental dynamic analysis. Soil Dynamics and Earthquake Engineering 104:432–436.

65. Karthik R, Jamie P, Reginald D (2015) Temporal evolution of seismic fragility curves for concrete box-girder bridges in California Engineering. Structures 97:29–46.

66. Alielahi H, Moghadam MR (2017) Fragility curves evaluation for broken-back block quay walls. Journal of Earthquake Engineering 21(1):1–22.

67. Pang R, Xu B, Zhou Y, Zhang X, Wang XL (2020) Fragility analysis of high CFRDs subjected to mainshock-aftershock sequences based on plastic failure. Engineering Structures 206:110152.

68. Dimova SL, Hirata K (2015) Simplified seismic fragility analysis of structures with two types of friction devices. Earthquake Engineering & Structural Dynamics 29(8):1153–1175.

69. Pang R, Xu B, Zou DG, Kong XJ (2018) Seismic performance assessment of high CFRDs based on fragility analysis. Science China Technological Sciences 61(4):635–648.

70. Xu B, Pang R, Zhou Y (2020) Verification of stochastic seismic analysis method and seismic performance evaluation based on multi-indices for high CFRDs. Engineering Geology 264:105412.

71. Wang ZY, Pedroni N, Zentner I, Zio E (2018) Seismic fragility analysis with artificial neural networks: Application to nuclear power plant equipment. Engineering Structures 162: 213–225.

72. Hu HQ, Huang Y, Chen ZY (2019) Seismic fragility functions for slope stability analysis with multiple vulnerability states. Environmental Earth Sciences 78:690.

73. Zhang W, Han L, Feng L, Ding X, Wang L, Chen Z, et al. (2020) Study on seismic behaviors of a double box utility tunnel with joint connections using shaking table model tests. Soil Dynamics and Earthquake Engineering 136:106118.